Advanced treatment of biologically pretreated coal chemical industry wastewater using the catalytic ozonation process combined with a gas-liquid-solid internal circulating fluidized bed reactor

Zhipeng Li, Feng Liu, Hong You, Yi Ding, Jie Yao and Chao Jin

ABSTRACT

This paper investigated the performance of the combined system of catalytic ozonation and the gas-liquid-solid internal circulating fluidized bed reactor for the advanced treatment of biologically pretreated coal chemical industry wastewater (CCIW). The results indicated that with ozonation alone for 60 min, the removal efficiency of chemical oxygen demand (COD) could reach 34%.

The introduction of activated carbon, pumice, γ-Al_2O_3 carriers improved the removal performance of COD, and the removal efficiency was increased by 8.6%, 4.2%, 2%, respectively. Supported with Mn, the catalytic performance of activated carbon and γ-Al_2O_3 were improved significantly with COD removal efficiencies of 46.5% and 41.3%, respectively; however, the promotion effect of pumice supported with Mn was insignificant. Activated carbon supported with Mn had the best catalytic performance. The catalytic ozonation combined system of MnO_X/activated carbon could keep ozone concentration at a lower level in the liquid phase, and promote the transfer of ozone from the gas phase to the liquid phase to improve ozonation efficiency.

Key words | advanced treatment, biologically pretreated, catalytic ozonation, coal chemical industry wastewater, gas-liquid-solid internal circulating fluidized bed reactor

Zhipeng Li
Feng Liu
Hong You (corresponding author)
Jie Yao
State Key Laboratory of Urban Water Resource and Environment,
Harbin Institute of Technology,
Harbin 150090,
China
E-mail: *youhong@hit.edu.cn*

Zhipeng Li
Feng Liu
Hong You
School of Marine Science and Technology,
Harbin Institute of Technology at Weihai,
Weihai 264209,
China

Yi Ding
Marine College, Shandong University at Weihai,
Weihai 264209,
China

Chao Jin
Department of Systems Design Engineering,
University of Waterloo,
Waterloo N2 L 3G1,
Canada

INTRODUCTION

A typical coal chemical industry wastewater (CCIW) contains a wide variety of organic contaminants from coking, coal gasification, and many other production and maintenance operations; some of the contaminants are present in high concentrations and are not removed by the conventional biological wastewater treatment processes (Zhuang *et al.* 2014; Jia *et al.* 2015; Zhuang *et al.* 2015). Nowadays, most existing chemical industry wastewater treatment plants are hard pressed to meet the increasingly stringent effluent discharge limits (Marulanda & Bolanos 2010). There is also an urgent need to recycle well-treated effluents for many beneficial reuse purposes but a much smaller fraction of industrial effluents are recycled and/or reused (Gogate & Pandit 2004). Therefore, the development of innovative wastewater treatment processes is essential for recycling chemical plant effluents (Ghose 2002).

Currently, coal chemical wastewater is widely treated by the anaerobic-anoxic-oxic (A^2/O) process, but the effluent has high color, nitrogen, chemical oxygen demand (COD), and contains many harmful and persistent organics, so it is difficult to meet the discharge standards (Kim & Ihm 2011). Through advanced treatment, the hazardous materials in the effluent could be effectively removed, and the effluent quality could meet standards. Then the reuse rate of coal chemical wastewater would be increased, which would have a great ecological and economic significance (Zhang *et al.* 2008).

Of the advanced treatment processes, ozonation in particular has attracted significant interest in the past decades because of its superior efficiency in refractory organics removal (Andreozzi *et al.* 1999). Heterogeneous catalytic ozonation can produce highly reactive hydroxyl radical

doi: 10.2166/wst.2018.073

oxidation (·OH), which non-selectively and quickly degrades all kinds of refractory organic pollutants in wastewater (Li & Qu 2009; Li *et al.* 2010; Wu *et al.* 2016). Heterogeneous catalytic ozonation can remove phenol and cyanide, reduce the COD value and improve biodegradability (Kepa *et al.* 2008; Vallet *et al.* 2013). Therefore, heterogeneous catalytic ozonation has received much attention for the degradation and mineralization of refractory organic pollutants due to its high effectiveness (He *et al.* 2010; Fajardo *et al.* 2013).

Gas-liquid-solid fluidized-bed systems have been applied extensively to chemical and biochemical processes because of their inherent advantages of enhanced mass transfer, improved interphase contact efficiency, and ease of handling large quantities of particles (Chowdhury *et al.* 2009). Compared to the conventional liquid-solid fluidized bed, the liquid-solid circulating fluidized bed has additional advantages (Zhu *et al.* 2000). Particles are entrained upwards in the riser fluidized bed, and then, after quick separation at the riser top, flow down into the downer fluidized bed. The liquid-solid circulating fluidized bed integrates two fluidized beds into one unit with the particles recirculating between the two fluidized beds (Chowdhury *et al.* 2009). Moreover, the circulating fluidized bed appears to have an important application value in environmental protection and process engineering for its simple structure and low energy consumption (Fan *et al.* 2008). Therefore, in this study, the heterogeneous catalytic ozonation process combined with gas-liquid-solid internal circulating fluidized bed reactor (GLSICFBR) has been proposed.

In previous studies, a wide variety of catalytic materials based on transition metal oxides were frequently used, such as manganese oxide (Zhao *et al.* 2014a), titanium oxide (Yang *et al.* 2007), zinc oxide (Gharbani & Mehrizad 2014), nickel oxide (Qin *et al.* 2009; Zhang *et al.* 2009), copper oxide (Petre *et al.* 2013), cerium oxide and iron oxide (Beltrán *et al.* 2005; Ciccotti *et al.* 2015). The application of catalytic ozonation required the development of highly efficient catalysts that had stable support materials to avoid the leaching of materials into the liquid system. Various materials were frequently used as catalyst support such as ceramic (Zhao *et al.* 2014b), silica (Rodríguez *et al.* 2014), zeolites (Petre *et al.* 2013), resins (Liotta *et al.* 2009), alumina (Al_2O_3) (Ikhlaq *et al.* 2012, 2013), and activated carbon (AC) (Cao *et al.* 2014). Ideal support materials should have characteristics of long durability, excellent mechanical strength, and high thermostability in the GLSICFBR.

This study focused on the performance of the combined system of the heterogeneous catalytic ozonation with GLSICFBR for advanced treatment of biologically pretreated CCIW. Activated alumina (γ-Al_2O_3), pumice, and AC were selected as catalyst carriers. The performance of these carriers supported with Mn were compared to choose the best carrier and catalyst of the combined system. The influence of catalyst on ozone (O_3) utilization rate was studied. The catalytic stability of AC was further confirmed in the catalytic ozonation process.

MATERIAL AND METHODS

Design and experimental setup of the combined system

The experimental installation of the combined system of the heterogeneous catalytic ozonation with GLSICFBR is shown in Figure 1. The experimental unit included three

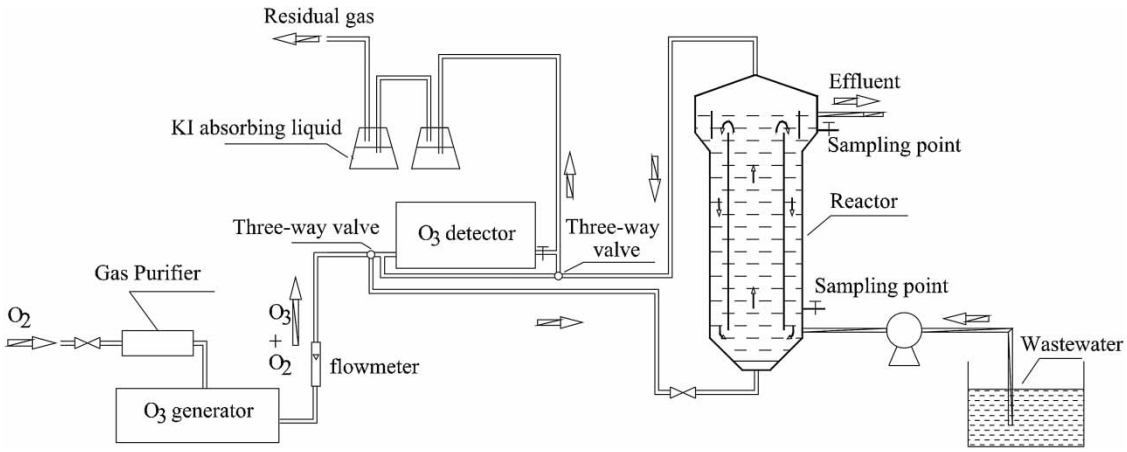

Figure 1 | Experimental equipment of the combined system of the heterogeneous catalytic ozonation with GLSICFBR.

parts: the preparation and quantification system of ozone, the ozone oxidation reactor, the concentration measurement and emission system of the remaining ozone. The preparation and quantification system of ozone consisted of the gas source, O_3 generator, gas flow and O_3 concentration detector. The production of O_3 was calculated by measuring the air flow rate and O_3 concentrations.

The core of the catalytic oxidation system is the inner circulating reactor with an effective volume of 4.0 L. In this study, the conventional fluidized bed reactor was divided into riser and downer fluidized bed through the baffle. The gas and liquid drove the cycle of the catalyst in the riser and downer areas. Catalysts were entrained upwards in the riser fluidized bed by a stream of wastewater having a velocity higher than the terminal velocity of the catalysts, and then, after a quick separation at the riser top and downflow into the downer, flowed downwards counter-currently with a stream of upwards wastewater in the downer fluidized bed, where the liquid velocity was lower than the terminal velocity. The inner circulating reactor thus integrated two fluidized beds into one unit and two processes could be held in one single system, with the catalysts recirculating between the two fluidized beds.

Gas-liquid-solid recirculation was beneficial to the chemical processes, greatly improving the update rate of the gas-liquid on the catalyst surface, and accelerating the process of heterogeneous catalysis. The O_3 completely mixed with the wastewater in the riser fluidized bed through the porous aeration, and then the wastewater during the flowing process carried the dissolved O_3 to the downer fluidized bed. The dissolved O_3 could react with the wastewater, which lowered the O_3 concentration re-entering the rising zone in the wastewater. The different O_3 concentrations between the riser and downer areas made the reactor improve the overall mass transfer efficiency and O_3 utilization in comparison with the conventional fluidized bed.

The effects of important operating parameters on the catalytic activity had been evaluated in our preliminary test. The addition of MnO_X/AC enhanced the pollutant removal performance. When dosing MnO_X/AC in the range from 0.0 to 1.5 g/L, the total organic carbon (TOC) removal efficiency increased faster than in the range from 1.5 to 2.5 g/L. The TOC removal efficiency at 1.5 g/L of MnO_X/AC was 31%. However, no significant differences were observed when the dose of MnO_X/AC increased from 1.5 to 2.5 g/L. Thus, the optimal amount of catalyst of 1.5 g/L was a tradeoff between efficient catalytic activity and cost.

As expected, TOC removal was enhanced with increasing temperature in the heterogeneous catalytic ozonation process. However, the need to control temperature means more operational costs in real application, therefore the raw wastewater temperature (20 °C) was used in this work.

Catalyst preparation

In this study, the activated alumina (γ-Al_2O_3), pumice, AC were chosen as catalyst carriers. The mean particle size of the carrier is 0.4 mm. These carriers were washed with deionized water, and then dried for 24 hours in an oven at 105 °C. Three kinds of catalysts were prepared by impregnation: MnO_X/γ-Al_2O_3, MnO_X/pumice, MnO_X/AC.

Preparation of MnO_X/γ-Al_2O_3: a certain amount of γ-Al_2O_3 carrier was placed in the 500 mL of 1 mol/L Mn $(NO_3)_2$ solution, which was timely shaken and stirred to remove air bubbles. After 24 hours, the immersion liquid was removed by filtration, and the solid was dried at 105 °C. The impregnation γ-Al_2O_3 was calcined at 500 °C in a muffle furnace for 3 hours. The preparation method of MnO_X/pumice was the same as the preparation of MnO_X/γ-Al_2O_3. The calcination method of MnO_X/AC was different to that of MnO_X/γ-Al_2O_3. The AC was calcined in a tubular furnace with a nitrogen protection, and the intake rate of nitrogen was about 50 cm^3/min. The temperature was set at 450 °C, and the calcination time was 3 hours.

Main characteristics of biologically pretreated CCIW

The real biologically pretreated CCIW used in this study was collected from the effluent of the secondary settling tank in the full-scale wastewater treatment facility. The wastewater had been treated with the A^2O process. The main characteristics of the real biologically pretreated CCIW were as follows: 100–150 mg/L COD, 0.05–0.08 BOD_5/COD ratio (B/C), 80–120 mg/L total phenol, 20–50 mg/L TOC, 60–70 mg/L total nitrogen (TN), and 35–50 mg/L of NH_4^+-N, 20–40 times of color. The pH ranged between 6.5 and 8.0.

Ozonation shows its advantage in color removal. It is found that decolorization was more than 80% after the first 60 min ozonation while the COD and TOC removal rate only reached 34% and 18%, respectively.

It is noteworthy that the catalytic ozonation process for completely eliminating pollutants is expensive because the oxidation intermediates formed during treatment tend to

be more and more resistant to chemical degradation (Muñoz *et al.* 2005). Nitrogen compounds were difficult to remove in the catalytic ozonation process (Yang *et al.* 2011). This study was focused on improving the COD and TOC removal efficiencies during the ozonation process. Therefore, the TOC and COD was the major analysis target, and the TN, NH_4^+ and color were not analyzed in this study.

Analytical method

The concentration of residual ozone in aqueous solution was measured by spectrophotometer using the indigo method (Bader & Hoigne 1981). Specific surface area, pore volume, and pore size were analysed by using a Micromeritics ASAP-2020 instrument. The catalyst morphology and element components were observed by using a Hitachi S-4700 scanning electron microscope (SEM) attached to an energy-dispersive X-ray (EDX) spectroscope. Nissan crystal analysis was investigated by using X-ray diffraction (XRD): Cu Kα radiation target, wavelength of 0.15418 nm, graphite monochromator, tube voltage 40 kV, current 150 mA, scan range 10–90°, and step length 0.02°.

TOC was determined with a TOC analyzer (TOC-V, Shimadzu Corporation, Japan). UV absorbance at 254 nm (UV_{254}) was determined by using a spectrometer (UV-2550, Shimadzu, Japan). COD, biochemical oxygen demand (BOD_5), and total phenol were measured by *Standard Methods* (APHA 1998).

RESULTS AND DISCUSSION

Characterization of the catalysts used in the combined system

The specific surface area (Brunauer–Emmett–Teller, BET) analysis

The specific surface area is an important factor affecting catalytic activity. The specific surface area, pore volume and pore size of the carriers and the carriers supported with MnO_X were determined, as shown in Table 1. The pumice had honeycomb pores, which were mostly large holes. But the inner pores were fewer compared to the other two carriers, so it was not suitable as a catalyst carrier. AC exhibited much higher specific surface area than the surface area of the γ-Al_2O_3 and pumice, and the pore volume of AC changed little after being supported with MnO_X. The surface of the AC supported with MnO_X was moderate, microporous, and not obviously bounded by the MnO_X.

Table 1 | BET results of the three carriers before and after being loaded with MnO_X

Sample	Specific surface area (m^2/g)	Pore volume (cm^3/g)	Pore size (A)
γ-Al_2O_3	249.0	0.401	61.35
MnO_X/γ-Al_2O_3	202.9	0.353	66.50
Pumice	0.946	0.001	44.04
MnO_X/pumice	2.952	0.005	64.61
AC	854.7	0.410	19.18
MnO_X/AC	779.6	0.361	19.11

Surface morphology (SEM)

Catalyst surface morphology can affect catalytic performance. In order to visually study the catalyst surface morphology, SEM and EDX analysis were conducted. The research results of pumice, MnO_X/pumice, AC, MnO_X/AC, γ-Al_2O_3, MnO_X/γ-Al_2O_3 are shown in Figure 2. It can be seen from Figure 2 (A-a1) and 2(B-a1) that the pumice surface contained a variety of crystals, which were irregularly arranged. Meanwhile, many types of elements had been found on the pumice surface, such as C, O, Si, Na, Mg, Al, K, Ca, Ti, Fe, etc. As seen from Figure 2 (A-a2) and 2(B-a2), the surface morphology of pumice supported with MnO_X changed greatly. This may have been caused by the dissolution of certain substances during the soaking stage. It was also possible to change the crystal shape and composition of some crystals on the surface under high temperature. The pumice has effectively supported by MnO_X, and the content of Mn was obviously higher than other elements.

As indicated by Figure 2(A-b1) and 2(B-b1), the surface of coconut shell AC has a well-developed pore structure. After being supported with MnO_X (Figure 2(A-b2) and 2(B-b2)), the pore size on the AC surface increased. The surface and inner holes were effectively filled with Mn, but the pore blockage was not serious. The crystalline state MnO_X appeared on the AC surface. In combination with BET analysis, Mn was effectively supported on the AC surface.

It was shown from Figure 2(A-c1) and 2(B-c1) that the crystals of the γ-Al_2O_3 surface were irregularly arranged and loose, while the pore size was uneven on the γ-Al_2O_3 surface. After being supported with MnO_X (Figure 2(A-c2) and 2(B-c2)), the surface morphology of γ-Al_2O_3 changed little. There were obvious MnO_X crystals on the γ-Al_2O_3

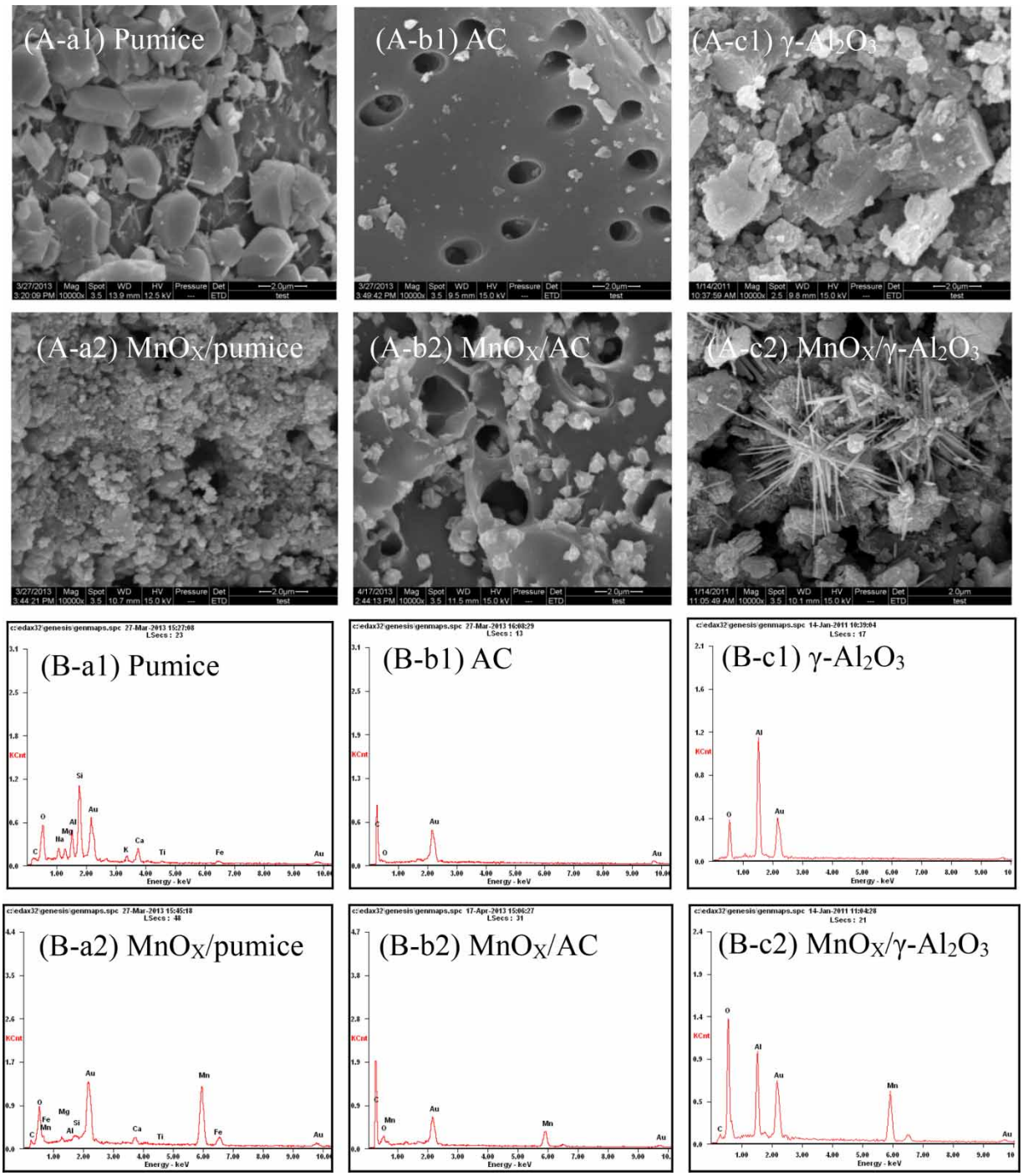

Figure 2 | SEM (A) and EDX (B) images of pumice (a), AC (b) and γ-Al_2O_3 (c) before (1) and after (2) being supported with MnO_X.

surface, and the quantity of crystals in the pores of the γ-Al_2O_3 was relatively higher. It was indicated from energy spectrum analysis that the MnO_X had been significantly supported on the surface of γ-Al_2O_3.

X-ray diffraction analysis

To analyse the crystal structure of pumice, AC, γ-Al_2O_3 supported with MnO_X, the crystal structure of the three carriers

and the carriers supported with Mn was analysed by XRD, as shown in Figure 3.

It can be seen from Figure 3(a) that there was no obvious characteristic diffraction peak in the XRD diagram of pumice and pumice supported with MnO_X, although the MnO_X had been observed on the pumice from the energy spectrum analysis. It may be due to the complexity of the elements and the crystal structure on the surface of pumice, which cause interference to the characteristic peaks of the pumice supported with MnO_X.

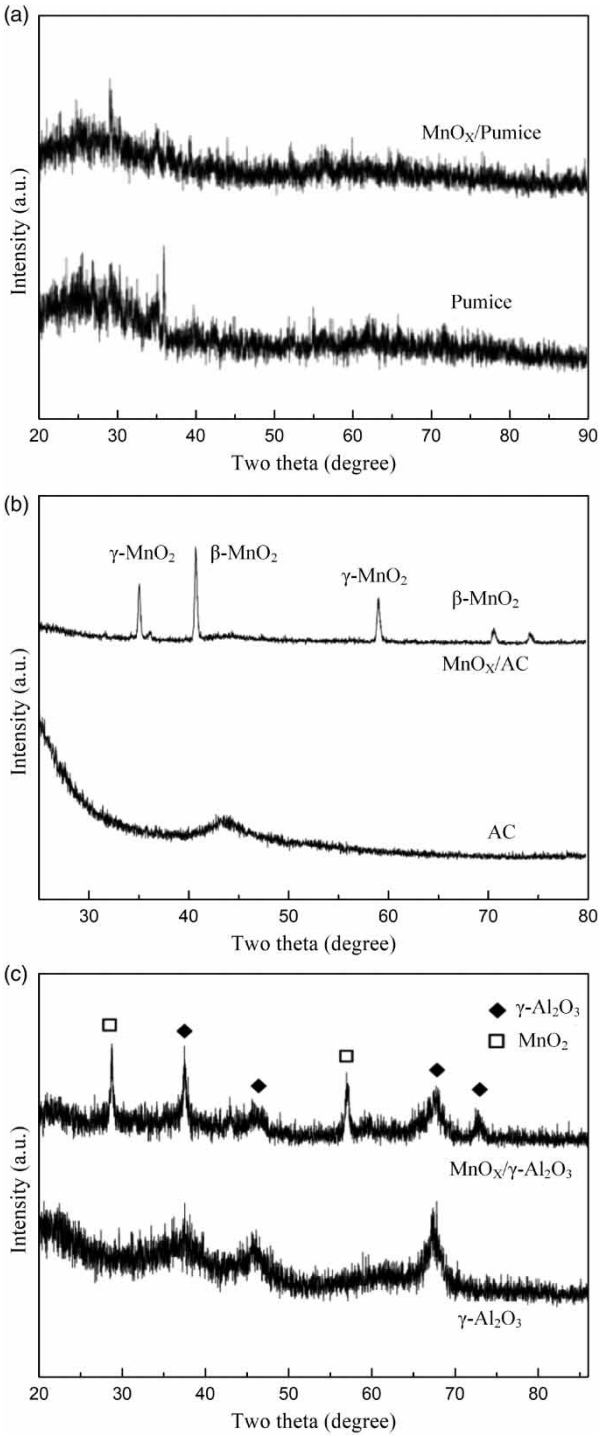

Figure 3 | XRD spectrum of pumice (a), AC (b) and γ-Al_2O_3 (c) before and after being supported with MnO_X.

The XRD diagram of AC and AC supported with MnO_X are shown in Figure 3(b). It was found that there was no characteristic peak on the surface of AC. For the AC supported with MnO_X, the diffraction angle (2 theta) appeared at 35.2 and 58.8 degrees, which were attributed to γ-MnO_2, and the characteristic peaks of β-MnO_2 appeared at 40.07 and 73.92 degrees. It was therefore demonstrated that the MnO_X supported on AC was mainly in the form of mixed crystals of MnO_2.

The XRD diagrams of γ-Al_2O_3 and γ-Al_2O_3 supported with MnO_X are shown in Figure 3(c). The XRD diagram of γ-Al_2O_3 mainly showed the characteristic diffraction peak of γ-Al_2O_3. After being supported with MnO_X, the diffraction angle (2 theta) showed a characteristic diffraction peak of γ-MnO_2 at about 28 and 58 degrees. The result indicated that the Mn had been effectively supported on the γ-Al_2O_3.

The catalytic performance of carriers supported with MnO_X in the combined system

Ozonation alone, ozonation with carriers and ozonation with catalysis experiments were performed. For the ozonation process with carriers, the ozonation performance of wastewater was compared, and the results are shown in Figure 4. The experimental conditions were: ozone concentration 17 mg/L, inlet velocity of air 40 L/h, and dosage of carriers 1.5 g/L.

It could be observed that in the system with single ozonation for 60 min, the removal efficiency of COD and TOC could reach 34% and 18%, respectively, and the ratio of BOD_5/COD increased from 0.085 to 0.35.

The addition of three carriers increased the removal efficiency of COD and TOC. The ratio of BOD_5/COD was 0.4, 0.38, 0.36 for the addition of AC, pumice, and γ-Al_2O_3, respectively. For the ozonation process with AC, the treatment performance was the best among the three carriers. It could be that the adsorption of AC played an important role in the removal of COD and greatly improved the final removal efficiency. The role of γ-Al_2O_3 on ozone catalytic oxidation has been demonstrated, and it has been widely used as catalyst carrier (Chen *et al.* 2015). By comparing COD and TOC removal, it was found that pumice could significantly accelerate the degradation rate. The specific surface area of pumice was

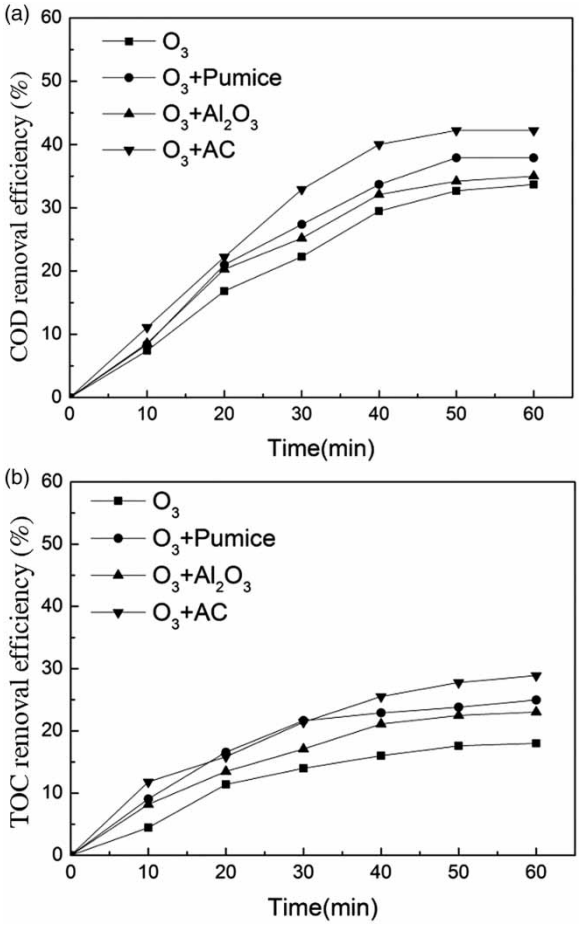

Figure 4 | The catalytic performance comparison of carriers before being loaded with MnO_X: (a) COD and (b) TOC.

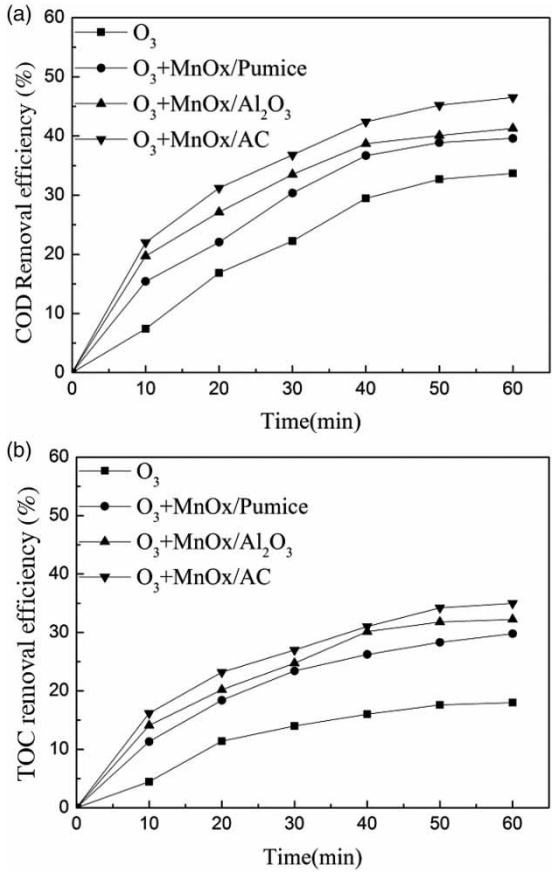

Figure 5 | The performance comparison of ozonation alone, ozonation with carriers and ozonation with catalysis: (a) COD and (b) TOC.

very small and the adsorption capacity of pumice was weak. Combined with the related characterization results, it could be seen that the catalytic performance of pumice was probably due to the large amount of metal oxide on its surface, which played a certain role in promoting the degradation effects.

After being supported with Mn, the catalytic ozonation performance of $MnO_X/\gamma\text{-}Al_2O_3$, MnO_X/pumice and MnO_X/AC was compared, and the results are shown in Figure 5. As illustrated in Figure 5, after being supported with Mn, the catalytic ozonation properties of MnO_X/AC and $MnO_X/\gamma\text{-}Al_2O_3$ had been obviously improved, however, the effect of pumice supported with Mn on ozonation was low. The ratio of BOD_5/COD was 0.40, 0.38, 0.45 for the addition of $MnO_X/\gamma\text{-}Al_2O_3$, MnO_X/pumice and MnO_X/AC, respectively. For the MnO_X/AC and $MnO_X/\gamma\text{-}Al_2O_3$, the removal efficiency of COD increased obviously at the beginning stage. The reaction time when the COD removal efficiency reached 30% for the MnO_X/AC and $MnO_X/\gamma\text{-}Al_2O_3$, was reduced by 9 min and 12 min, respectively. Reaction rate was visibly accelerated and reaction time was shortened by the addition of the catalyst. When the COD removal efficiency was stable, the removal efficiency with MnO_X/AC addition increased by 5% compared with that with $MnO_X/\gamma\text{-}Al_2O_3$ addition. The TOC removal efficiency was 4% higher for MnO_X/AC compared with that for $MnO_X/\gamma\text{-}Al_2O_3$. After being supported with Mn, AC had better catalytic performance than the other two carriers supported with Mn, because of its high specific surface area and outstanding adsorption ability. After being supported with Mn, the specific surface area of AC decreased, but the removal efficiency was improved. It was known that the increased efficiency of MnO_X/AC system was due to the catalytic effect after being supported with Mn.

Pumice catalytic performance did not change significantly after being supported with MnO_X. The main reason was probably due to pumice's lower specific surface area and adsorption capacity. Meanwhile, the SEM analysis showed that the shape and size of the surface crystal changed significantly after being supported with Mn, which

might be caused by the decomposition of inorganic salt on the surface under high temperature. These results indicated that pumice was not suitable as catalyst carrier.

In addition, it was found that after being supported with Mn, the density of AC was still low and it was easy to flow compared to the MnO_X/γ-Al_2O_3 catalysts. It was suitable for internal circulating fluidized bed reactor. Hence, the system with MnOx/AC has the advantages of increased liquid-solid contact efficiency and enhanced mass transfer. Therefore, it was better to use MnO_X/AC as catalyst for catalytic ozonation of coal chemical wastewater in the combined system than MnO_X/γ-Al_2O_3 catalysts. AC has been extensively used as an efficient catalyst and catalyst support with distinguished characteristics of high surface area, chemical resistance and adsorption capacity (Faria *et al.* 2007). However, the catalytic activity and stability of AC should be further confirmed in catalytic ozonation process.

The influence of AC catalyst on ozone utilization rate in the combined system

The effect of AC catalyst (MnO_X/AC) on the ozone utilization rate in the treatment of coal chemical wastewater by ozone oxidation was investigated. Under conditions with and without catalyst, the concentration of ozone in the intake and exhaust gas was measured by an ozone concentration meter during the coal chemical wastewater treatment process.

Control experiments were carried out with deionized water. When the ozone concentration in the tail gas was stable, the ozone generator was switched off. The gas drum was continuously operated to remove the ozone from the liquid phase. The ozone concentration recording was stopped until the ozone concentration was 0 mg/L. The result is shown in Figure 6. It was assumed that once the ozone was absorbed into the water, it could react with the pollutants. The ozone quantity that did not dissolved in the reactor and decompose by itself was neglected. After fitting the curves, the change of ozone utilization in the process was calculated by integral calculation, as shown in Table 2.

In the control test, few substances in water reacted with ozone. Therefore, the major process was ozone dissolution. The ozone dissolution rate of the first 10 min decreased slowly. The main reason was that the concentration of ozone in water increased continuously, which led to the increase of mass transfer resistance. At the 13th min, the ozone dissolution reached equilibrium, and the ozone concentration was about 2.5 mg/L. The ozone dynamic absorption rate was close to zero, thereafter, the ozone concentration in liquid phase remained in dynamic equilibrium. At 20 min, the ozone generator was switched off, and the ozone in the water was stripped by the air. The concentration of ozone in the tail gas decreased rapidly to 0 mg/L. The total amount of exhaust gas in the whole process was stable, and it was basically consistent with the air intake. After fitting the curves, the calculated content of total ozone absorption in the first 20 min and blowing out after 20 min were 114.38 mg and 110 mg, respectively. The results showed that the amount of ozone self-decomposition

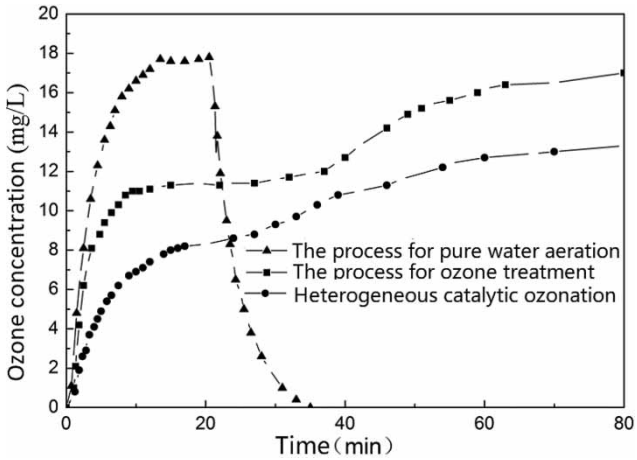

Figure 6 | Residual ozone concentration in tail gas with and without catalyst during the coal chemical wastewater treatment process.

Table 2 | The absorption and utilization rate of ozone under different conditions

	The absorption rate of pure water (%)		The utilization rate of ozone in wastewater (without catalyst) (%)		The utilization rate of ozone in wastewater (with MnO_X/AC) (%)	
Time (min)	Instant	Total	Instant	Total	Instant	Total
0	–	–	–	–	–	–
2	86.36	93.09	96.47	98.09	97.06	98.00
5	63.64	82.93	72.35	88.70	87.06	94.00
10	27.27	59.10	45.88	76.17	74.18	85.60
15	5.68	36.39	34.71	70.02	59.41	74.40
20	≈0	27.39	34.12	62.75	52.94	68.00
30	≈0	16.39	33.53	54.09	48.80	64.20
40	–	–	31.76	46.68	45.30	59.33
50	–	–	25.29	42.34	36.04	56.00
60	–	–	11.76	33.74	30.25	51.52

was less during the experiment. In conclusion, the ozone transfer rate and utilization rate could be estimated by the amount of intake and output ozone.

The ozone concentration in the tail gas during the coal chemical wastewater treating process without catalyst is shown in Figure 6 and Table 2. Ozone transfer and utilization could be broadly divided into three stages: rapid utilization, uniform utilization and deceleration utilization. In the first 10 min, the transfer efficiency of ozone to wastewater was very high, which was significantly higher than that in the control experiment at the same time point. This higher transfer efficiency was determined by the ozone transfer from the gas phase to the liquid phase and the ozone reaction with organic compounds in water. After 10 min, the ozone concentration in liquid phase did not reach the value of the ozone concentration in liquid measured during dissolution balance in the control experiment. It showed that the organic compounds in the liquid phase were continuously consuming dissolved ozone, resulting in a low concentration of ozone in the system. At 20–40 min, the instantaneous utilization rate was maintained at about 30–33%, and the ozone concentration in the tail gas concentration was kept at 11–12 mg/L. The ozone transfer rate was approximately equal to the ozone utilization rate. The ozone concentration in water was about 0.02–0.07 mg/L with a trend of gradually increasing, but the concentration was lower than that of the control. It was indicated that the ozone was quickly utilized when the ozone entered the liquid phase from the gas phase. Under the experimental conditions, the stage of 0–40 min was the main stage of the reaction of ozone with the pollutants in water. The results were consistent with the changes in the pollutant removal curves in the previous experiments. But with the reaction proceeding, the instantaneous transfer rate decreased rapidly after 40 min. The primary reason was that the pollutant concentration which could react with ozone was reduced, and the ozone requirement was reduced, which led to the increase of the ozone concentration in liquid phase, the mass transfer resistance and the ozone concentration in the tail gas.

As shown in Figure 6 and Table 2, the change of ozone concentration in the tail gas after adding MnO_X/AC catalyst was analysed. When the catalyst was added, the ozone instantaneous transfer efficiency increased to 48.8% at 20 min, which was 13.3% higher than that without catalyst. The ozone concentration in liquid phase with catalyst system was lower than that without catalyst system at the same time. The change of ozone concentration in tail gas showed that ozone catalytic oxidation also had three stages: fast utilization, uniform utilization and deceleration utilization. After 60 min, the efficiency of ozone transfer was stable, which was lower than that without catalyst system. It showed that the catalyst could speed up the ozone transfer, keep the ozone concentration in the liquid phase at a low level, and increase the ozone utilization ratio. Based on the previous experimental results, it was proved that MnO_X/AC had obvious capability of adsorption and catalytic oxidation. Through the investigation of the ozone utilization rate, it could provide a reference for the continuous flow experiment in the future, and guide the ozone dosage through the change of ozone utilization rate, so as to make the process more economical.

The stability of AC catalyst in the combined system

In order to investigate the stability of MnO_X/AC, the catalyst was reused for catalytic treatment of coal chemical wastewater. After each use, the catalyst was recovered, rinsed with deionized water, and dried at 80 °C. After being used five times, the removal effects of TOC and UV_{254} were

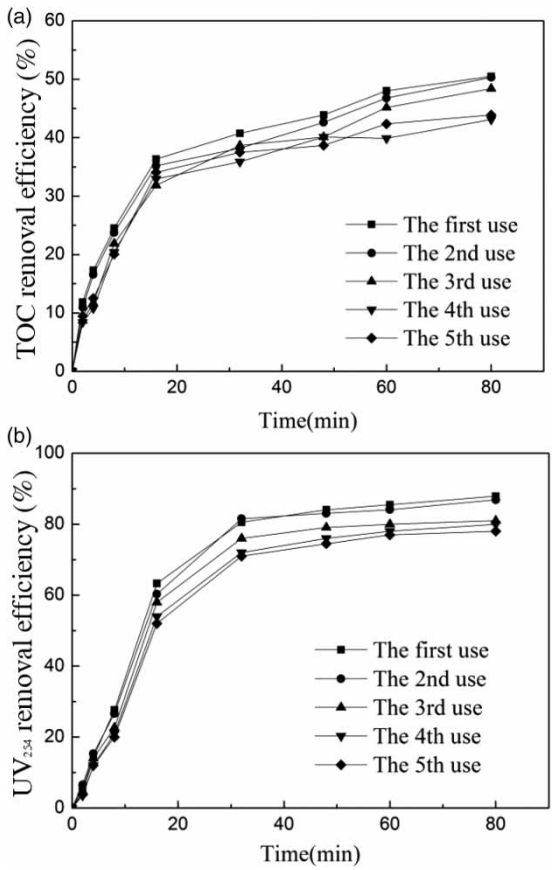

Figure 7 | Catalytic performance of MnO_X/AC with the reuse process: (a) TOC and (b) UV_{254}.

investigated, as shown in Figure 7. As illustrated by Figure 7, the removal efficiency of TOC and UV_{254} showed little change, indicating that the catalyst has obvious catalytic activity after continuous use. Taking into account the error caused by the catalyst loss in the recovery process, it was proved that the catalyst was stable and suitable for wastewater treatment.

CONCLUSION

The combined system of catalytic ozonation and the GLSICFBR was devised for advanced treatment of biologically pretreated CCIW. Pumice, γ-Al_2O_3 and AC were chosen as catalysis carriers for catalytic ozonation in the GLSICFBR. AC had the highest specific surface area among the three carriers, and changed little after being supported with Mn. Meanwhile, XRD analysis suggested that MnO_X/AC had obvious characteristic diffraction peaks of MnO_2. Compared with other catalysts, the catalytic performance of MnO_X/AC improved significantly with the removal efficiency of COD and TOC reaching 46.5% and 35.0%. The MnO_X/AC catalyst could speed up the transfer of ozone to other substances, keep the ozone concentration in the liquid phase at a low level, and promote the transfer of ozone from the gas phase to the liquid phase, thus increasing the utilization ratio. Although the catalytic activity decreased 10–20% after being repeatedly used, taking into account the loss of catalyst in the recovery process, the MnO_X/AC showed a stable performance in the combined system.

ACKNOWLEDGEMENTS

This study was supported by the National Natural Science Fund of China (No. 51408158), the China Postdoctoral Science Foundation (No. 2017M612278), Natural Science Foundation of Shandong Province of China (No. ZR2017MEE020 and ZR2017PEE008), the Fundamental Research Funds for the Central Universities (No. HIT. NSRIF.2016098) and the scientific research foundation of Harbin institute of technology at Weihai (HIT(WH)201403).

REFERENCES

Andreozzi, R., Caprio, V., Insola, A. & Marotta, R. 1999 Advanced oxidation processes (AOP) for water purification and recovery. *Catalysis Today* **53**, 51–59.

APHA 1998 *Standard Methods for the Examination of Water and Wastewater*, 20th edn. American Public Health Association, American Water Works Association, Water Environment Federation, Washington, DC.

Bader, H. & Hoigne, J. 1981 Determination of ozone in water by the indigo method. *Water Res.* **15**, 449–456.

Beltrán, F. J., Rivas, F. J. & Montero-de-Espinosa, R. 2005 Iron type catalysts for the ozonation of oxalic acid in water. *Water Research* **39**, 3553–3564.

Cao, H., Xing, L., Wu, G., Xie, Y., Shi, S., Zhang, Y., Minakata, D. & Crittenden, J. C. 2014 Promoting effect of nitration modification on activated carbon in the catalytic ozonation of oxalic acid. *Applied Catalysis B: Environmental* **146**, 169–176.

Chen, C., Yoza, B. A., Wang, Y., Wang, P., Li, Q. X., Guo, S. & Yan, G. 2015 Catalytic ozonation of petroleum refinery wastewater utilizing Mn-Fe-Cu/Al_2O_3 catalyst. *Environmental Science & Pollution Research* **22**, 5552–5562.

Chowdhury, N., Zhu, J., Nakhla, G., Patel, A. & Islam, M. 2009 A novel liquid-solid circulating fluidized-bed bioreactor for biological nutrient removal from municipal wastewater. *Chemical Engineering & Technology* **32**, 364–372.

Ciccotti, L., do Vale, L., Hewer, T. & Freire, R. 2015 Fe_3O_4@TiO_2 preparation and catalytic activity in heterogeneous photocatalytic and ozonation processes. *Catalysis Science & Technology* **5**, 1143–1152.

Fajardo, A. S., Martins, R. C. & Quinta-Ferreira, R. M. 2013 Treatment of a simulated phenolic effluent by heterogeneous catalytic ozonation using Pt/Al_2O_3. *Environmental Technology* **34**, 301–311.

Fan, L., Xu, N., Zhang, Y. & Shi, H. 2008 Structure optimization of an improved inner-Circulating biological fluidized Bed by numerical simulation. *Environmental Engineering Science* **25**, 839–848.

Faria, P. C. C., Órfão, J. J. M. & Pereira, M. F. R. 2007 Ozonation of aniline promoted by activated carbon. *Chemosphere* **67**, 809–815.

Gharbani, P. & Mehrizad, A. 2014 Heterogeneous catalytic ozonation process for removal of 4-chloro-2-nitrophenol from aqueous solutions. *Journal of Saudi Chemical Society* **18**, 601–605.

Ghose, M. K. 2002 Complete physico-chemical treatment for coke plant effluents. *Water Research* **36**, 1127–1134.

Gogate, P. R. & Pandit, A. B. 2004 A review of imperative technologies for wastewater treatment I: oxidation technologies at ambient conditions. *Advances in Environmental Research* **8**, 501–551.

He, Z., Zhang, A., Song, S., Liu, Z., Chen, J., Xu, X. & Liu, W. 2010 γ-Al_2O_3 modified with praseodymium: an application in the heterogeneous catalytic ozonation of succinic acid in aqueous solution. *Industrial & Engineering Chemistry Research* **49**, 12345–12351.

Ikhlaq, A., Brown, D. R. & Kasprzyk-Hordern, B. 2012 Mechanisms of catalytic ozonation on alumina and zeolites in water: formation of hydroxyl radicals. *Applied Catalysis B: Environmental* **123**, 94–106.

Ikhlaq, A., Brown, D. R. & Kasprzyk-Hordern, B. 2013 Mechanisms of catalytic ozonation: an investigation into

superoxide ion radical and hydrogen peroxide formation during catalytic ozonation on alumina and zeolites in water. *Applied Catalysis B: Environmental* **129**, 437–449.

Jia, S., Han, H., Zhuang, H., Xu, P. & Hou, B. 2015 Advanced treatment of biologically pretreated coal gasification wastewater by a novel integration of catalytic ultrasound oxidation and membrane bioreactor. *Bioresource Technology* **189**, 426–429.

Kepa, U., Stanczyk-Mazanek, E. & Stepniak, L. 2008 The use of the advanced oxidation process in the ozone plus hydrogen peroxide system for the removal of cyanide from water. *Desalination* **223**, 187–193.

Kim, K. H. & Ihm, S. K. 2011 Heterogeneous catalytic wet air oxidation of refractory organic pollutants in industrial wastewaters: a review. *Journal of Hazardous Materials* **186**, 16–34.

Li, D. & Qu, J. 2009 The progress of catalytic technologies in water purification: a review. *Journal of Environmental Sciences* **21**, 713–719.

Li, B., Xu, X., Zhu, L., Ding, W. & Mahmood, Q. 2010 Catalytic ozonation of industrial wastewater containing chloro and nitro aromatics using modified diatomaceous porous filling. *Desalination* **254**, 90–98.

Liotta, L., Gruttadauria, M., Di Carlo, G., Perrini, G. & Librando, V. 2009 Heterogeneous catalytic degradation of phenolic substrates: catalysts activity. *Journal of Hazardous Materials* **162**, 588–606.

Marulanda, V. & Bolanos, G. 2010 Supercritical water oxidation of a heavily PCB-contaminated mineral transformer oil: laboratory-scale data and economic assessment. *J Supercrit Fluid* **54**, 258–265.

Muñoz, I., Rieradevall, J., Torrades, F., Peral, J. & Domènech, X. 2005 Environmental assessment of different solar driven advanced oxidation processes. *Solar Energy* **79**, 369–375.

Petre, A., Carbajo, J., Rosal, R., Garcia-Calvo, E. & Perdigón-Melón, J. 2013 Cuo/SBA-15 catalyst for the catalytic ozonation of mesoxalic and oxalic acids. water matrix effects. *Chemical Engineering Journal* **225**, 164–173.

Qin, W., Li, X. & Qi, J. 2009 Experimental and theoretical investigation of the catalytic ozonation on the surface of NiO – CuO nanoparticles. *Langmuir* **25**, 8001–8011.

Rodríguez, J. L., Valenzuela, M. A., Tiznado, H., Poznyak, T. & Flores, E. 2014 Synthesis of nickel oxide nanoparticles supported on SiO_2 by sensitized liquid phase photodeposition for applications in catalytic ozonation. *Journal of Molecular Catalysis A: Chemical* **392**, 39–49.

Vallet, A., Ovejero, G., Rodriguez, A., Peres, J. A. & Garcia, J. 2013 Ni/MgAlO regeneration for catalytic wet air oxidation of an azo-dye in trickle-bed reaction. *Journal of Hazardous Materials* **244**, 46–53.

Wu, J., Ma, L., Chen, Y., Cheng, Y., Liu, Y. & Zha, X. 2016 Catalytic ozonation of organic pollutants from bio-treated dyeing and finishing wastewater using recycled waste iron shavings as a catalyst: removal and pathways. *Water Research* **92**, 140–148.

Yang, Y., Ma, J., Qin, Q. & Zhai, X. 2007 Degradation of nitrobenzene by nano-TiO_2 catalyzed ozonation. *Journal of Molecular Catalysis A: Chemical* **267**, 41–48.

Yang, S., Wang, Q., Zhang, T., Li, P. & Wu, C. 2011 Biological nitrogen removal using the supernatant of ozonized sludge as extra carbon source. *Ozone Science & Engineering* **33**, 410–416.

Zhang, H., Changqing, D., Lei, B. & Qian, Z. 2008 Experiment study on corrosion control using coking wastewater as circulating cooling water. *Earth Science Frontiers* **15**, 186–189.

Zhang, X., Li, X. & Qin, W. 2009 Investigation of the catalytic activity for ozonation on the surface of NiO nanoparticles. *Chemical Physics Letters* **479**, 310–315.

Zhao, H., Dong, Y., Jiang, P., Wang, G., Zhang, J., Li, K. & Feng, C. 2014a An α-mno_2 nanotube used as a novel catalyst in ozonation: performance and the mechanism. *New Journal of Chemistry* **38**, 1743–1750.

Zhao, L., Ma, W., Ma, J., Yang, J., Wen, G. & Sun, Z. 2014b Characteristic mechanism of ceramic honeycomb catalytic ozonation enhanced by ultrasound with triple frequencies for the degradation of nitrobenzene in aqueous solution. *Ultrasonics Sonochemistry* **21**, 104–112.

Zhu, J. X., Karamanev, D. G., Bassi, A. S. & Zheng, Y. 2000 (Gas-) liquid-solid circulating fluidized beds and their potential applications to bioreactor engineering. *Canadian Journal of Chemical Engineering* **78**, 82–94.

Zhuang, H., Han, H., Jia, S., Hou, B. & Zhao, Q. 2014 Advanced treatment of biologically pretreated coal gasification wastewater by a novel integration of heterogeneous catalytic ozonation and biological process. *Bioresource Technology* **166**, 592–595.

Zhuang, H., Han, H., Ma, W., Hou, B., Jia, S. & Zhao, Q. 2015 Advanced treatment of biologically pretreated coal gasification wastewater by a novel heterogeneous Fenton oxidation process. *Journal of Environmental Sciences* **33**, 12–20.

First received 18 October 2017; accepted in revised form 6 February 2018. Available online 20 February 2018